AIP | Journal of Applied Physics

Valence force field-based Monte Carlo bond-rotation method for the determination of sp2-bonded carbon structures

Sangheon Lee and Gyeong S. Hwang

Citation: J. Appl. Phys. **110**, 093524 (2011); doi: 10.1063/1.3660383
View online: http://dx.doi.org/10.1063/1.3660383
View Table of Contents: http://jap.aip.org/resource/1/JAPIAU/v110/i9
Published by the American Institute of Physics.

Valence force field-based Monte Carlo bond-rotation method for the determination of sp^2-bonded carbon structures

Sangheon Lee and Gyeong S. Hwang[a)]
Department of Chemical Engineering, University of Texas, Austin, Texas 78712, USA

(Received 27 June 2011; accepted 8 October 2011; published online 15 November 2011)

We present a valence force field (VFF)-based Monte Carlo (MC) bond-rotation method capable of identifying stable sp^2-bonded carbon configurations. The VFF contains four parameters that are adjusted to fit density functional theory (DFT) calculations for both planar and non-planar model structures; the simple VFF model is shown to reliably reproduce the DFT energetics of disordered sp^2-bonded carbon with various topologies and sizes. The MC bond-rotation method combined with the VFF is demonstrated to be effective in determining minimum-energy sp^2-bonded carbon structures, such as topological defects and fullerenes with different sizes. The computational approach is also applied to investigate possible configurations of multi-vacancy defects (V_{2n}, $2 \leq n \leq 8$) and their relative stability. © *2011 American Institute of Physics*. [doi:10.1063/1.3660383]

I. INTRODUCTION

sp^2-bonded carbon nanostructures in various dimensions (0 D fullerenes, 1 D nanotubes, 2 D graphene nanosheets, and 3 D porous carbon with negative curvature) possess unique and remarkable properties. Over the past decades, great attention has been drawn toward understanding the nature and characteristics of nanostructured carbon materials and exploring their potential application in a variety of mechanical,[1] electronic,[2] optoelectronic,[3] and energy storage devices.[4–6] In particular, the unique ability of carbon networks to reorganize the atomic structure and accordingly modify the properties makes the study of nanostructured carbon very rich and intriguing. Ion, electron, and photon irradiation methods[7,8] have been recently employed to tailor carbon nanostructures, for instance, through creation of small topological defects,[9] nanoribbons,[10] dislocations,[8] and grain boundaries.[11] However, the local atomic configurations of disordered carbons are not yet fully clarified, despite their importance in understanding and manipulating relevant properties; this is due in part to the difficulty of direct characterization. Until relatively recently, atomic-scale imaging of the structure of carbons would have been hardly achievable, although transmission electron microscopy (TEM) would seem to be an ideal tool. Given that computational approaches can be a powerful and flexible alternative.

In recent years, increased efforts have been undertaken to develop structural models for sp^2-bonded carbon using various computational techniques including *ab initio* structural relaxation,[12–16] tight-binding molecular dynamics (MD),[17–20] and classical force-field methods.[21–23] First principles methods permit an accurate description of atomic arrangements, but are quite limited in the number of atoms and time scale they can handle. Classical MD simulations with empirical force fields can deal with relatively large systems, but still suffer from time scale limitations that could hamper complete structural relaxation, particularly for strong network lattices of covalently-bonded carbon atoms.

Previous experimental studies[8,24–26] have shown that sp^2-bonded carbon may undergo structure rearrangements under irradiation at high temperatures without creation of a noticeable amount of undercoordinated atoms. This implies that the carbon lattices can be well represented by fully-coordinated networks, which has also been supported by earlier first principles calculations.[12,17] In addition, there is general agreement that the structural transformation between different configurations may occur predominantly via successive C-C bond rotations, the so-called Stone-Wales (SW) bond rotations.[27] This may suggest that thermodynamically favored structural models could be obtained through comparisons of the energetics of possible trivalent structures generated by a series of SW bond rotations. A natural choice of computational method to implement this idea would be Metropolis Monte Carlo (MMC).[28] Moreover, the MMC approach does not involve bond formation/scission such that a computationally less expensive force field model can be used, which in turn permits simulation of large systems.

In this paper, we present a MC bond-rotation scheme based on a simple but reliable valence force field (VFF) for determination of the structure and energetics of sp^2-bonded carbon structures. The VFF is parameterized to fit the energetics of various model structures from density functional theory (DFT) calculations. We evaluate how well the VFF calculates the structure and energetics of sp^2-bonded carbon through comparisons with DFT and other available force field (FF) models. We also apply the VFF-based MC method to investigate possible configurations for multi-vacancy defects (V_{2n}, $2 \leq n \leq 8$). The computational approach turns out to be very effective in identifying possible minimum-energy configurations of sp^2-bonded carbon (with no coordination defects), encompassing fullerenes, nanotubes, (corrugated) graphene nanosheets, and their hybrid structures with different types of topological defects.

[a)]Author to whom correspondence should be addressed. Electronic mail: gshwang@che.utexas.edu.

II. CALCULATION METHODS

A. Density functional theory

All DFT calculations herein were performed using the well-established plane wave program, VASP,[29] within the generalized gradient approximation of Perdew and Wang (GGA-PW91).[30] Vanderbilt-type ultrasoft pseudopotentials[31] were adopted to describe the interaction between ion cores and valence electrons. Valence electron wave-functions were expanded using a plane wave basis set with a kinetic-energy cut-off of 400 eV. All structures were fully-relaxed using the conjugate gradient method until residual forces on constituent atoms became smaller than 5×10^{-2} eV/Å. Brillouin-zone (BZ) sampling was performed using k-point meshes in the scheme of Monkhorst-Pack (M-P).[32]

B. Valence force field model and parameter determination

Within the VFF model, the energetics of sp^2-bonded carbon structures is evaluated in terms of the increase in energy with respect to the total C-C bond energy corresponding to a single sheet of graphite (referred to as graphene) in the ground state. Here, we adopted a four-parameter VFF model that takes into account the contributions of: (i) two-body bond stretching, (ii) three-body bond bending, (iii) four-body curvature-induced pyramidalization, and (iv) π-orbital misalignment between two adjacent carbon atoms. A more sophisticated VFF model[33] with six parameters has been developed particularly to describe the phonon properties of graphite and nanotubes; however, as demonstrated later the simplified four-parameter model turns out to be sufficient for the determination of the relative stability of carbon nanostructures that insignificantly deviate in bond topologies from the reference graphene structure.

Given the four-parameter model, we write the energy of sp^2-bonded carbon as

$$E = k_r r_0^{-2} \sum_{i,j\in i} (r_{ij} - r_0)^2 + k_\theta \sum_{i,j<k\in i} (\cos\theta_{ijk} - \cos\theta_0)^2 + k_\phi r_0^{-2} \sum_{i,j<k<l\in i} \left(\frac{3\vec{r}_{ij} \cdot \vec{r}_{ik} \times \vec{r}_{il}}{r_{ij}r_{ik} + r_{ik}r_{il} + r_{il}r_{ij}} \right)^2 + k_\varphi \sum_{i,j\in i} \left| \vec{\pi}_i \times \vec{\pi}_j \right|^2, \quad (1)$$

where k_r, k_θ, k_ϕ, and k_φ are adjustable parameters to be determined, the subscripts ij, ik, il, and ijk represent pairs and triplets involving atoms i, j, k, and l (while j, k, and l are the three neighbors of i), r_{ij} is the interatomic distance between atoms i and j, and θ_{ijk} is the angle between bonds ij and ik. Here, $\vec{r}_{ij} = \vec{r}_i - \vec{r}_j$ where $\vec{r}_i$ is the atomic position vector of atom i, and $\cos\theta_{ijk}$ and π_i are defined as

$$\cos\theta_{ijk} = \frac{\vec{r}_{ij} \cdot \vec{r}_{ik}}{r_{ij}r_{ik}},$$

$$\vec{\pi}_i = 3\frac{\vec{r}_{ij} \times \vec{r}_{ik} + \vec{r}_{ik} \times \vec{r}_{il} + \vec{r}_{il} \times \vec{r}_{ij}}{r_{ij}r_{ik} + r_{ik}r_{il} + r_{il}r_{ij}}. \quad (2)$$

Note that in the summations double counting of triple interactions is avoided.[33]

The four parameters (k_r, k_θ, k_ϕ, k_φ) were adjusted to fit DFT-GGA calculations in the following sequence that corresponds to an increase in the degrees of freedom of each training set: (1) k_r; (2) k_θ; and (3) k_ϕ and k_φ; training sets employed in parameter optimization are illustrated in Fig. 1. The best-fit parameters are listed in Table I, which were obtained through minimization of the cross-validation error

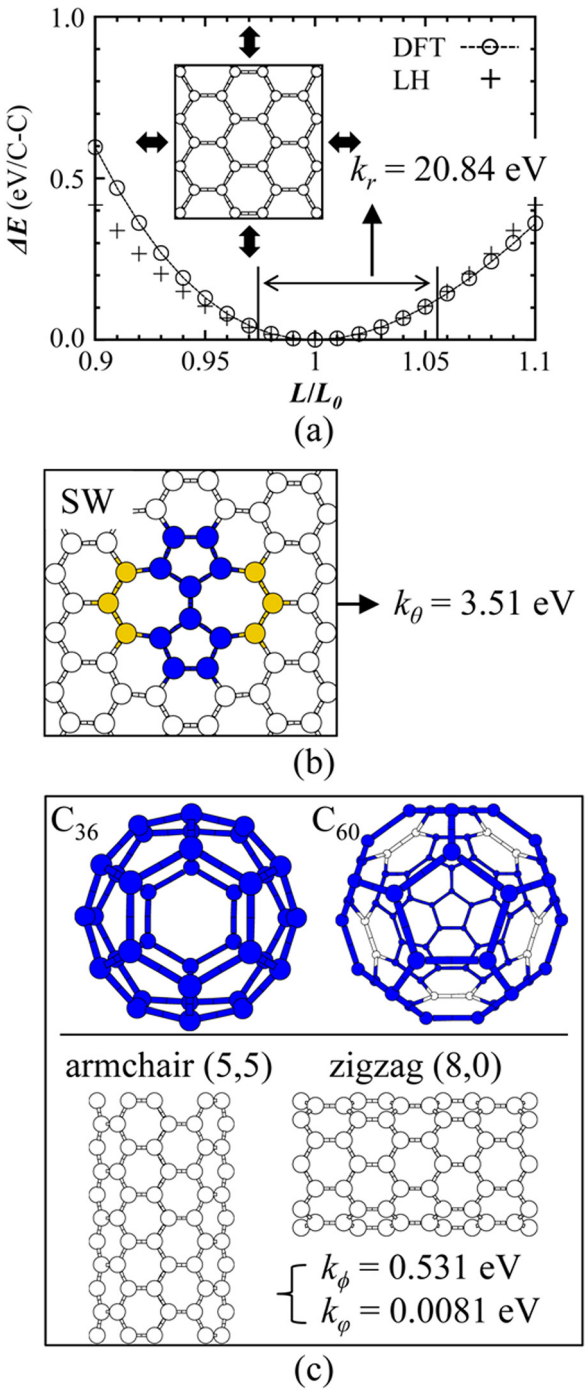

FIG. 1. (Color online) Training sets used in parameter optimization: (a) k_r from energy variation (per C-C bond) with respect to lattice constant in graphene; (b) k_θ from Stone-Wales (SW) defect in graphene; and (c) k_ϕ and k_φ from two different sizes of fullerene (C_{36} and C_{60}) and two different nanotube structures [armchair (5, 5) and zigzag (8, 0)]. Black (blue) filled circles represent atoms comprising 5-membered rings, gray (gold) filled circles are atoms included in 7-membered rings but not in 5-membered rings, and unfilled circles indicate the rest of the lattice atoms.

(ξ) given by $\xi^2 = \frac{1}{N}\sum_{n=1}^{N}(E_{DFT}^{(n)} - E_{VFF}^{(n)})^2$, where $E_{DFT}^{(n)}$ and $E_{VFF}^{(n)}$ refer to the DFT and VFF energies, respectively, of the nth of N total models in the training set; the energies were evaluated based on fully-relaxed structures (with the same network) from each calculation.

For the GGA value of $r_0 = 1.424$ Å (and the hexagon interior angle of $\theta_0 = 120°$), k_r was first optimized based on the total energy variation of graphene as a function of lattice constant (−2% to 5%) [see Fig. 1(a)], and then k_θ was adjusted to match the formation energy of a single Stone-Wales (SW) defect that is made by a 90° degree in-plane rotation of a C-C bond about its center [Fig. 1(b)]; the resulting pentagons and heptagons have interior angles varying from 100° to 141°. For the DFT calculations, we used a 4-atom supercell for the lattice constant variation and a 288-atom (6×12 unit cells) supercell for the SW defect formation energy; the respective Brillouin-zone (BZ) integrations were performed using $8 \times 12 \times 1$ and $2 \times 2 \times 1$ (Monkhorst-Pack) k-point meshes.

Next, we determined k_ϕ and k_φ simultaneously using two different sizes of fullerene (C_{36} and C_{60}) and two different nanotube structures [armchair (5, 5) and zigzag (8, 0)] [Fig. 1(c)]. The strain in nonplanar conjugated carbon structures arises from pyramidalization and π-orbital misalignment.[34] Very little π-orbital misalignment, if any, exists in fullerene structures; for instance, the π-orbitals of C_{60} are perfectly aligned.[35] Hence, the strain in fullerenes is predominantly caused by pyramidalization.[35] On the other hand, in the case of nanotubes π-orbital misalignment tends to be the main source of strain with a minor contribution of pyramidalization; for instance, the armchair (5, 5) structure consists of two types of C-C bonds with π-orbital misalignment angles of either $\varphi = 0°$ or 21.3°, while the pyramidalization angle of its sidewall is only $\phi \approx 6.0°$.[36] For the fullerene calculations, we employed a cubic periodic supercell of 20 Å sides (which is sufficiently large to avoid unphysical interactions with the periodic images. The periodic supercells for the armchair and zigzag nanotubes include 10 unit cells (corresponding to 2.47 nm long according to the DFT-GGA) and 6 unit cells (2.56 nm long) along the tube axis, respectively; the lateral separation between the (periodic image) tube centers is about 20 Å. Γ-point BZ sampling was used for the DFT calculations of both fullerenes and nanotubes.

C. Metropolis Monte Carlo

For a defective system, its atomic structure is allowed to evolve toward thermodynamic equilibrium though MC bond-rotation moves, as depicted in Fig. 2. Similar to the Wooten-Winer-Weaire (WWW) bond transposition scheme,[37] a bond-rotation move involves the breaking of two bonds (A-B and C-D) followed by the making of two new bonds (A-C and B-D). In a perfect hexagonal lattice, such bond-rotation leads to SW defect formation (where four adjacent hexagons are transformed into two pentagons and two heptagons). The acceptance or rejection of each bond-switching move is determined using probability $P = min[1, exp(-\Delta E/k_B T)]$, where ΔE is the energy difference between the old and the trial configuration; the old and trial structures were fully relaxed by the Polak and Ribiere's conjugate-gradient method.[38] Successive MC bond-rotation moves enable one to search all possible configurations of a sp^2-bonded carbon system, regardless of kinetic barriers associated.

TABLE I. Parameters of the valence force field model [Eq. (1), VFF(LH)] employed in this work, which were adjusted to fit DFT-GGA calculations. Units are in eV.

k_r	k_θ	k_ϕ	k_φ
20.84	3.51	0.531	0.0081

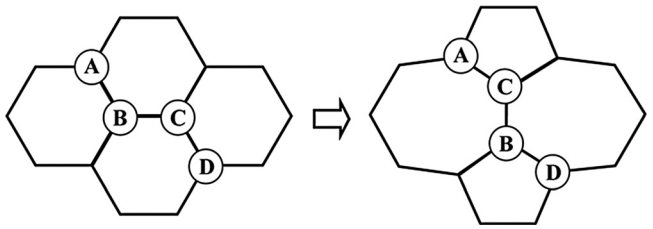

FIG. 2. Illustration of a MC bond-rotation move that involves the 90° rotation of a single bond (B-C) by breaking two bonds (A-B and C-D) and forming two new bonds (A-C and B-D); this bond rotation yields a Stone-Wales (SW) defect (right).

According to earlier theoretical calculations,[39,40] the barriers for C-C bond rotations are in the range of 4–10 eV, depending on the local atomic configuration. Given the large barriers, thermally-activated bond rotation appears to be infrequent under typical annealing conditions (< 1000 °C); however, the structural interconversion via the bond rotation mechanism is likely facilitated by moderate-energy electron irradiation. Very recently Kotakoski *et al.*[8] provided evidence that irradiation-induced topological defects can gradually undergo transformation into more stable configurations though successive bond rotations under continued electron-beam exposure (in which electron energies were just above the threshold for atom displacement). As demonstrated later our MC bond-rotation scheme combined with the four-parameter VFF model well describes the structural relaxation process and effectively determines the minimum-energy configurations of disordered (sp^2-bonded) carbon nanostructures of various dimensions.

III. RESULTS AND DISCUSSION

A. Comparison between VFF and DFT

We first evaluated the accuracy and reliability of the four-parameter VFF model [referred to as VFF(LH) hereafter to distinguish it from other VFF models] in calculation of the structure and energetics of sp^2-bonded carbon nanostructures, through comparisons with DFT-GGA results for (i) small topological defects in graphene, (ii) fullerenes, and (iii) nanotubes. For comparison, we also considered the more sophisticated (six-parameter) VFF model developed by Perebeinos and Tersoff [VFF(PT)][33] and the Brenner empirical bond-order-dependent FF [BOD-FF(BR)].[41]

The small topological defects considered include (i) Stone-Wales (SW or 5-7-7-5) [Fig. 2 (right)], (ii) 5-8-5,

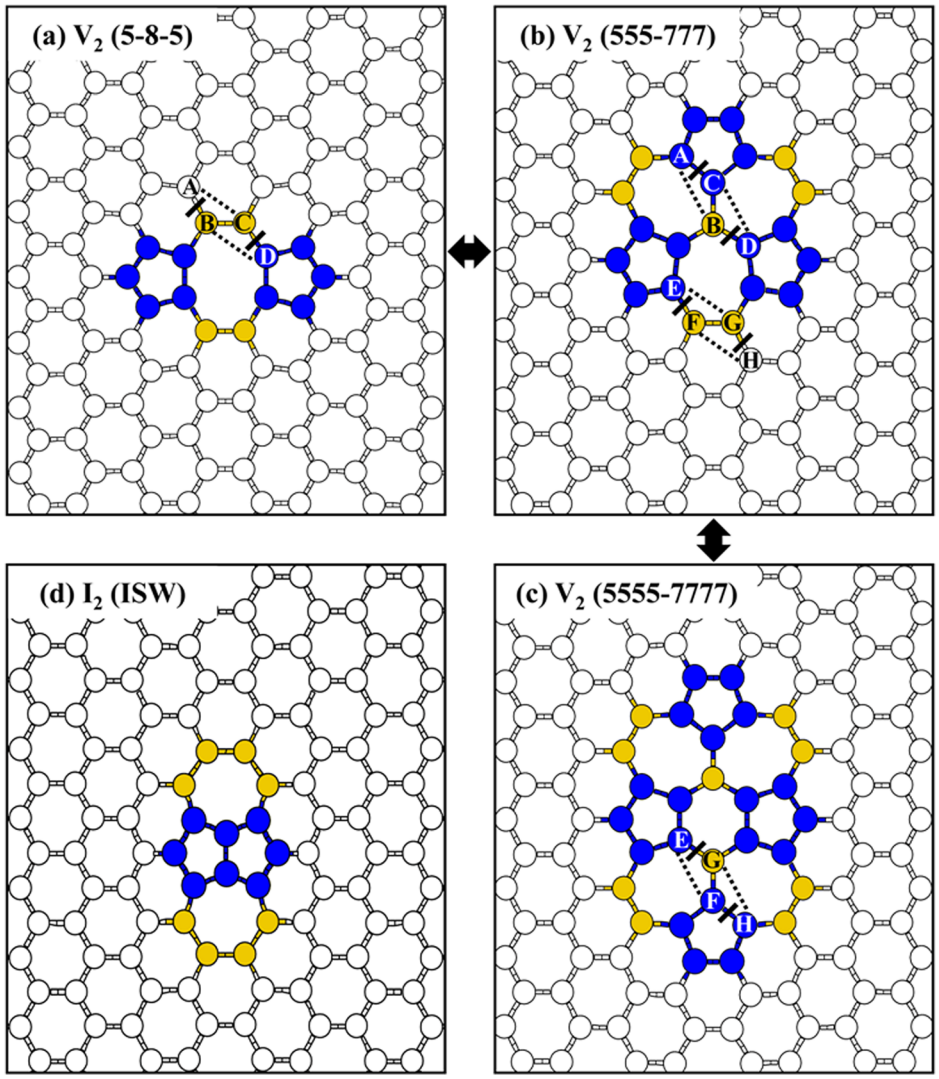

FIG. 3. (Color online) Di-vacancy (V_2) at different configurations (5-8-5, 555–777, and 5555–7777) and ISW di-interstitial (I_2), as indicated. The 5-8-5, 555–777, and 5555–7777 defects may undergo interconversion through bond rotations, as illustrated (- - - - and | indicate bond formation and break, respectively). Black (blue) filled circles represent atoms comprising 5-membered rings, gray (gold) filled circles are atoms included in 7-membered rings but not in 5-membered rings, and unfilled circles indicate the rest of the lattice atoms.

555–777, and 5555–7777 di-vacancies (V_2), and (iii) "inverse Stone-Wales (ISW or 7-5-5-7)" di-interstitial (I_2), as depicted in Figs. 2 and 3. The V_2 5-8-5, 555–777, and 5555–7777 defects may undergo interconversion via Stone-Wales bond rotations (see Fig. 3); while they all have been observed experimentally,[8,42] the 555–777 defect is likely to be the most energetically favorable form.[14,17] For the I_2 ISW defect, the formation of the abutting 5-membered rings and two 7-membered rings induces a strong local curvature. Our MMC simulations based on VFF(LH) consistently predicted the 555–777 and ISW defects to be thermodynamically the most probable V_2- and I_2-type defects, respectively, consistent with previous studies.[15,17] Fig. 4 summarizes the predicted formation energies of these small topological defects from DFT-GGA, VFF(LH), VFF(PT), and BOD-FF(BR) calculations. The formation energy (E_f) is given by: $E_f = E(N \pm n) - (1 \pm n/N)E'(N)$, where $E(N \pm n)$ represents the total energy of the N ($N+n$ or $N-n$)-atom supercell containing a single SW defect (n interstitials or vacancies) and $E'(N)$ is the N-atom pristine graphene total energy. Here, we used a supercell with $N = 288$ (corresponding to 6×12 unit cells), and an $(2 \times 2 \times 1)$ k-point M-P mesh for BZ sampling. Overall VFF(LH) yields the best agreement with DFT, while VFF(PT) and BOD-FF(BR) tend to overestimate the

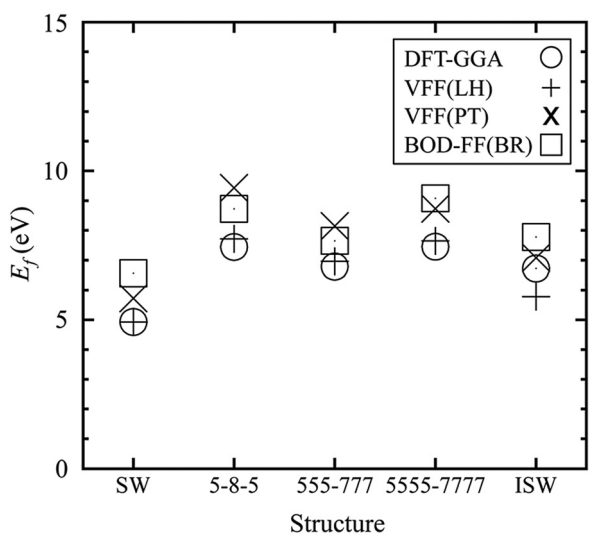

FIG. 4. Predicted formation energies (E_f) of small topological defects (SW, V_2, I_2, as depicted in Figs. 2 and 3) from DFT-GGA, VFF(LH), VFF(PT), and BOD-FF(BR) calculations.

formation energies except for the ISW defect; this is not surprising because VFF(LH) parameters were optimized based on DFT-GGA calculations.

Using VFF(LH)-based MMC simulations, we constructed even-numbered C_{2n} $(15 \le n \le 35)$ fullerenes; the MC bond-rotation approach turns out to be very effective in identification of possible fullerene configurations. Our simulations well reproduced the minimum-energy configurations of fullerenes with various sizes (including D_{6h} symmetry C_{36} in Ref. 43, truncated icosahedron (I_h) C_{60} in Ref. 44, and D_{5h} symmetry C_{70} in Ref. 45), while obeying the so-called isolated pentagon rule (IPR)[46,47] for large structures ($2n = 60$, 70, and $2n > 70$).

Figures 5 and 6 summarize the relative formation energies ($\hat{E}_f$ per carbon atom) of fullerenes and nanotubes with respect to defect-free graphene, which we obtained from DFT, VFF(LH), VF(PT), and BOD-FF(BR) calculations. Here, both (n, n) armchair and $(m, 0)$ zigzag nanotubes with different diameters ($n = 5$–9 and $m = 8$–12) were considered to examine the diameter and chirality dependences. $\hat{E}_f$ is calculated by $\{E(N) - E'(N)\}/N$, where $E(N)$ and $E'(N)$ refer to the total energies of N-atom fullerene (or nanotube) and pristine graphene, respectively. The conditions employed for the DFT and FF calculations are described in Sec. II. B. For a wide size range of both fullerenes and nanotubes, the DFT-GGA and VFF(LH) formation energies are in excellent agreement, whereas VFF(PT) and BOD-FF(BR) somewhat overestimate and underestimate the nanotube formation energies, respectively, and they both yield higher formation energies for fullerenes as compared to DFT-GGA. The quantitative agreement between VFF(LH) and DFT suggests that the simplified four-parameter model can be sufficient for determination of the structure and thermodynamic stability of sp^2-bonded carbon (that insignificantly deviates in bond lengths and bond angles from the ideal honeycomb lattice of graphene). However, we should point out that more sophisticated FF models such as VFF(PT) might be necessary to describe more rigorously the phonon dispersions and vibrational properties.

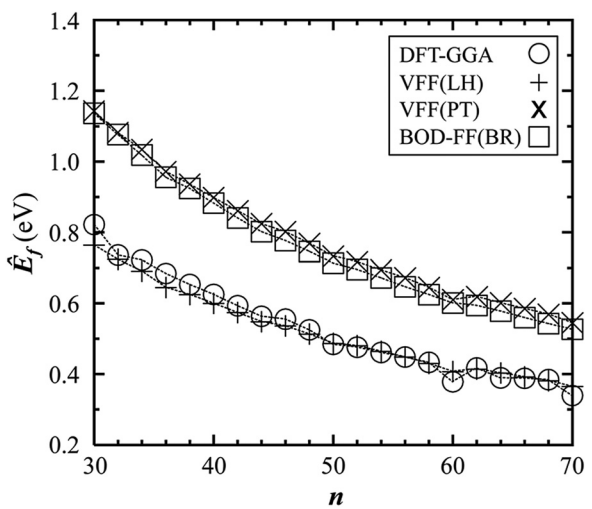

FIG. 5. Predicted relative formation energies per carbon atom ($\hat{E}_f$) of even-numbered fullerenes (C_{2n}, $15 \le n \le 35$) with respect to defect-free graphene from DFT-GGA, VFF(LH), VF(PT), and BOD-FF(BR) calculations. Here, the fullerene structures were obtained using the VFF(LH)-based MC bond-rotation method presented herein.

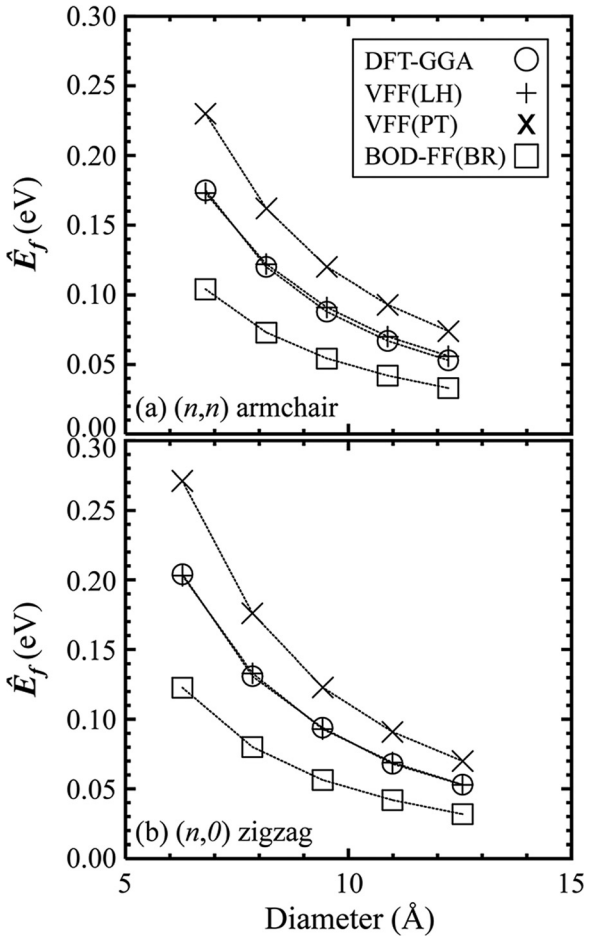

FIG. 6. Predicted relative formation energies per carbon atom ($\hat{E}_f$) of carbon nanotubes of two different chiralities and various sizes with respect to defect-free graphene from DFT, VFF(LH), VF(PT), and BOD-FF(BR) calculations; (a) (n, n) armchair ($n = 5$–9) and (b) $(m, 0)$ zigzag ($m = 8$–12) nanotubes.

B. Multi-vacancy structures in graphene

Vacancies are believed to be the predominant defects in graphene,[48,49] and can be created during growth or upon irradiation.[7,8] Monovacancies were naturally the first choice of study in earlier theoretical investigations[50] and transmission electron microscopy (TEM) experiments;[8,9] however, they may undergo migration with moderate activation energy (~1.7 eV) (Ref. 51) and agglomerate into vacancy clusters at elevated temperatures. The accurate determination of multi-vacancy structures is of great importance for a better understanding of the properties of defective graphene. Using the VFF(LH)-based MMC scheme, we investigated possible configurations for multi-vacancy defects (V_{2n}, $2 \le n \le 8$). Here, a relatively large $(6240 - 2n)$-atom supercell (corresponding to 30×52 unit cells with $2n$ vacancies) to avoid the unwanted interaction between periodic images.

In the size regime, our simulations consistently predicted that the minimum-energy structures are grouped into

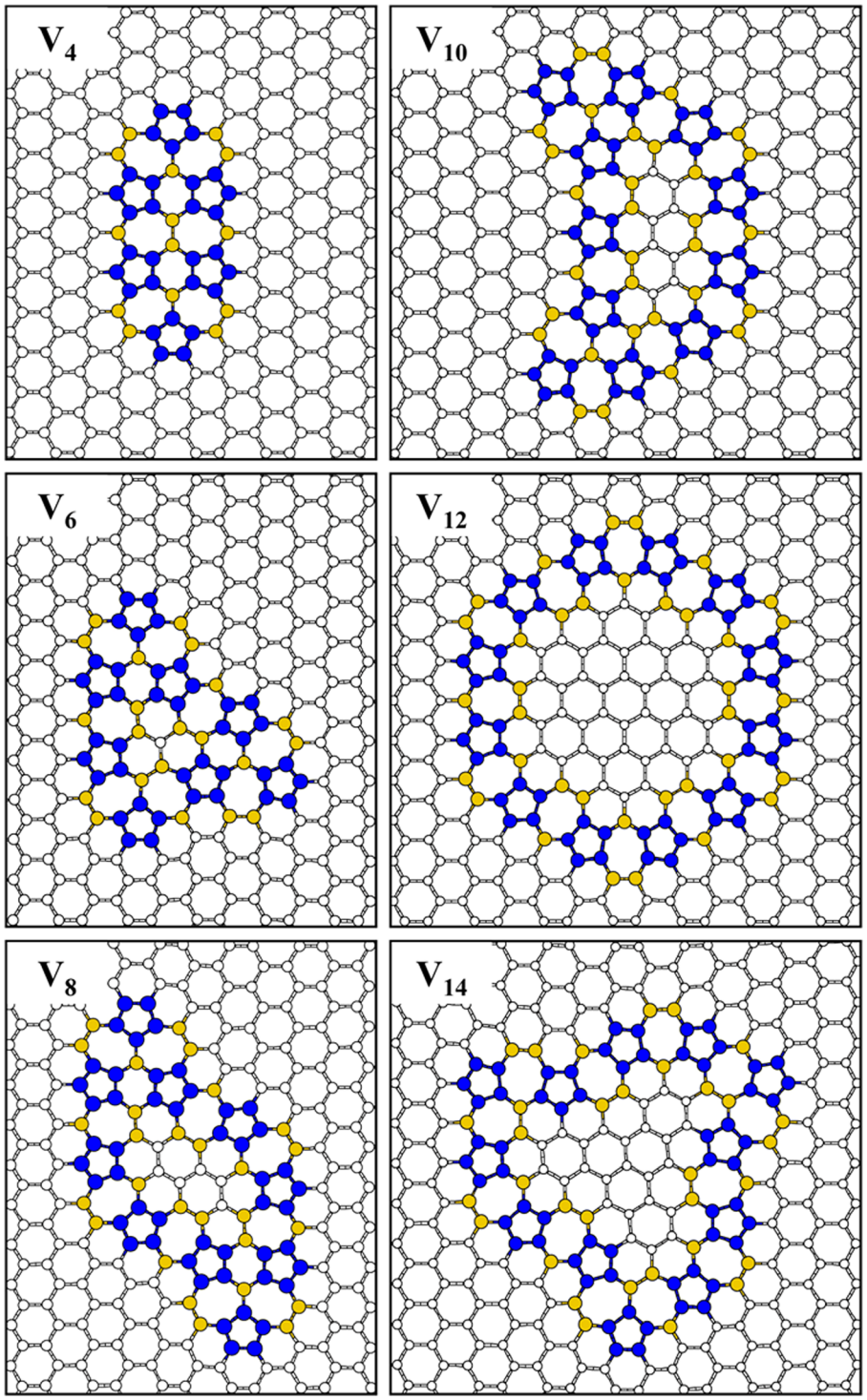

FIG. 7. (Color online) Minimum-energy configurations for loop-type vacancy defects (V_{2n}, $n = 2–7$) in graphene, calculated by the VFF(LH)-based MC bond-rotation method presented herein. Black (blue) filled circles represent atoms comprising 5-membered rings, gray (gold) filled circles are atoms included in 7-membered rings but not in 5-membered rings, and unfilled circles indicate the rest of the lattice atoms.

"loop" (see Fig. 7) and "dislocation" (see Fig. 8). The loop-type defect consists of a chain of alternating pentagons and heptagons that surrounds a cluster of hexagons (rotated by 30° with respect to the original lattice). As the number of vacancies increases, the inner hexagonal lattice becomes two-dimensional rather than elongated in one direction; interestingly, in V_{12} the 5–7 pairs can be favorably arranged to enclose a circular-shaped domain. Very recently, the formation of loop-type multi-vacancy defects was evidenced by HRTEM measurements.[8] In addition, the 5–7 chains tend to be a key building block for graphene grain boundaries, according to a recent CVD (chemical vapor deposition) growth study of graphene.[11] For each dislocation-type defect, there are two separated 5–7 pairs with different chirality; that is, a 5–7 defect (+ dislocation) and a 7–5 defect (− dislocation). The distance between the edge dislocation dipoles increases with increasing the number of vacancies; the dislocation structure has been rather well studied.[14,52] As summarized in Fig. 9, our VFF calculations predict that when less than twelve vacancies the loop structure is thermodynamically more stable than the dislocation structure while the larger clusters favor the dislocation type.

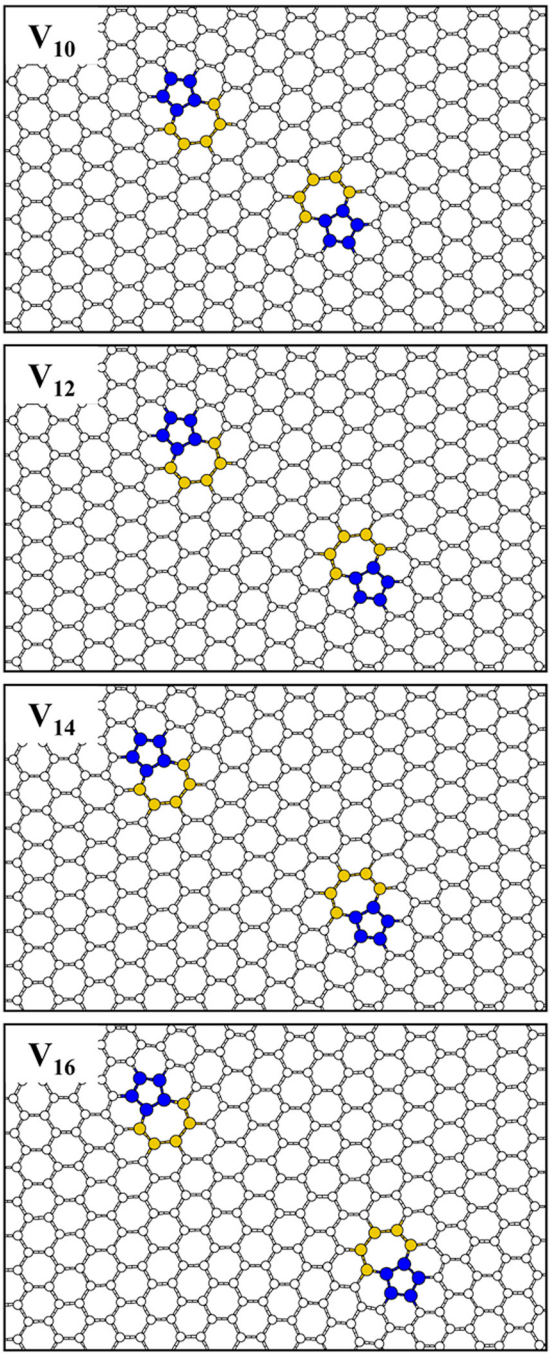

FIG. 8. (Color online) Minimum-energy configurations for dislocation-type vacancy defects (V_{2n}, n = 5–8) in graphene, calculated by the VFF(LH)-based MC bond-rotation method presented herein. Black (blue) filled circles represent atoms comprising 5-membered rings, gray (gold) filled circles are atoms included in 7-membered rings but not in 5-membered rings, and unfilled circles indicate the rest of the lattice atoms.

IV. SUMMARY

We developed a VFF-based MC bond-rotation scheme that can be applied to identify the minimum-energy configurations of sp^2-bonded carbon. We adopted a four-parameter VFF model that takes into account two-body bond stretching, three-body bond bending, four-body curvature-induced pyramidalization, and π-orbital misalignment between two adjacent carbon atoms. The parameters were adjusted to fit DFT-GGA results for both planar and non-planar model

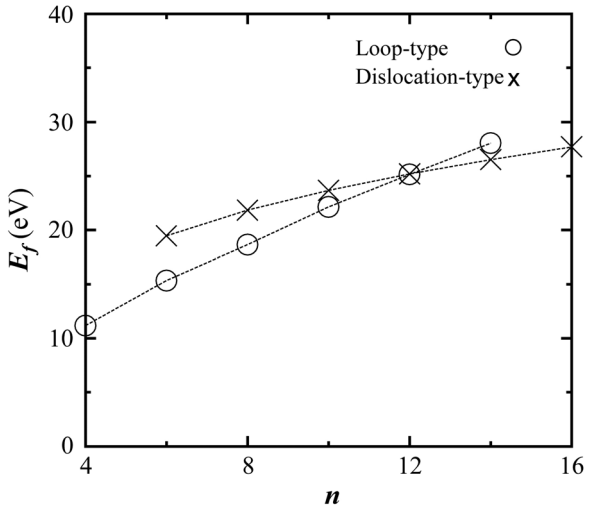

FIG. 9. Predicted formation energies (E_f) of loop-type (V_{2n}, $2 \le n \le 7$) and dislocation-type (V_{2n}, $3 \le n \le 8$) multi-vacancy defects.

structures. We demonstrated that the VFF very closely reproduces the DFT formation energies of small topological defects in graphene, fullerenes, and nanotubes; the quantitative agreement suggests that the simplified four-parameter model can be sufficient for evaluation of the thermodynamic stability of sp^2-bonded carbon (that insignificantly deviates in bond lengths and bond angles from the ideal honeycomb lattice of graphene). Combined with the simple but reliable VFF, the MC bond-rotation method consistently yielded the minimum-energy configurations of fullerenes with various sizes and small topological defects in graphene. This clearly demonstrates that this computation approach can be an effective way to identify possible sp^2-bonded carbon structures (free of coordination defects). Note that the current VFF model is only applicable to cases with no bond-coordination defect; however, it could further be improved by taking into account additional penalty energy terms associated with under- or over-coordinated C atoms to address their effects on the structural properties and energetics.[53] Finally, we applied this method to the study of multi-vacancy defects (V_{2n}, $2 \le n \le 8$) that render no under- or over-coordinated atoms. In this size regime, our simulations show that the vacancies tend to be grouped into loop- and dislocation-type defects; when less than twelve vacancies the loop structure is predicted to be thermodynamically more stable than the dislocation structure, while the larger clusters favor the dislocation type. We envision that the modeling effort will contribute to a better understanding of the structural properties of carbon-based materials, which will further provide valuable guidance on how to manipulate the carbon structure to achieve desired properties for specific applications including electronics, optoelectronics, energy storage, and sensors.

ACKNOWLEDGMENTS

This work was supported by the U.S. Department of Energy, Office of Basic Energy Sciences, Division of Materials Sciences and Engineering under Award ID DE-SC001951. We would also like to thank the Texas Advanced Computing Center for use of their computing resources.

[1]J. S. Bunch, A. M. van der Zande, S. S. Verbridge, I. W. Frank, D. M. Tanenbaum, J. M. Parpia, H. G. Craighead, and P. L. McEuen, Science **315**, 490 (2007).
[2]P. Avouris, Z. H. Chen, and V. Perebeinos, Nature Nanotech. **2**, 605 (2007).
[3]J. A. Misewich, R. Martel, P. Avouris, J. C. Tsang, S. Heinze, and J. Tersoff, Science **300**, 783 (2003).
[4]L. Schlapbach and A. Züttel, Nature **414**, 353 (2001).
[5]J. R. Miller, R. A. Outlaw, and B. C. Holloway, Science **329**, 1637 (2010).
[6]M. D. Stoller, S. Park, Y. Zhu, J. An, and R. S. Ruoff, Nano Lett. **8**, 3498 (2008).
[7]A. V. Krasheninnikov and K. Nordlund, J. Appl. Phys. **107**, 071301 (2010).
[8]J. Kotakoski, A. V. Krasheninnikov, U. Kaiser, and J. C. Meyer, Phys. Rev. Lett. **106**, 105505 (2011).
[9]A. Hashimoto, K. Suenaga, A. Gloter, K. Urita, and S. Iijima, Nature **430**, 870 (2004).
[10]R. Y. Oeiras, F. M. Araújo-Moreira, and E. Z. da Silva, Phys. Rev. B **80**, 073405 (2009).
[11]P. Y. Huang, C. S. Ruiz-Vargas, A. M. van der Zande, W. S. Whitney, M. P. Levendorf, J. W. Kevek, S. Garg, J. S. Alden, C. J. Hustedt, Y. Zhu, J. Park, P. L. McEuen, and D. A. Muller, Nature **469**, 389 (2011).
[12]J. M. Carlsson and M. Scheffler, Phys. Rev. Lett. **96**, 046806 (2006).
[13]S. Berber and A. Oshiyama, Phys. Rev. B **77**, 165405 (2008).
[14]B. W. Jeong, J. Ihm, and G.-D. Lee, Phys. Rev. B **78**, 165403 (2008).
[15]M.T. Lusk and L.D. Carr, Phys. Rev. Lett. **100**, 175503 (2008).
[16]K. E. Kweon and G. S. Hwang, Phys. Rev. B **82**, 195439 (2010).
[17]G.-D. Lee, C. Z. Wang, E. Yoon, N.-M. Hwang, D.-Y. Kim, and K. M. Ho, Phys. Rev. Lett. **95**, 205501 (2005).
[18]P. M. Ajayan, V. Ravikumar, and J.-C. Charlier, Phys. Rev. Lett. **81**, 1437 (1998).
[19]M. Terrones, F. Banhart, N. Grobert, J.-C. Charlier, H. Terrones, and P. M. Ajayan, Phys. Rev. Lett. **89**, 075505 (2002).
[20]A. V. Krasheninnikov, K. Nordlund, and J. Keinonen, Phys. Rev. B **66**, 245403 (2002).
[21]O. Lehtinen, J. Kotakoski, A. V. Krasheninnikov, A. Tolvanen, K. Nordlund, and J. Keinonen, Phys. Rev. B **81**, 153401 (2010).
[22]M. Yasuda, Y. Kimoto, K. Tada, H. Mori, S. Akita, Y. Nakayama, and Y. Hirai, Phys. Rev. B **75**, 205406 (2007).
[23]A. V. Krasheninnikov, K. Nordlund, and J. Keinonen, Phys. Rev. B **65**, 165423 (2002).
[24]J. H. Warner, M. H. Rummeli, L. Ge, T. Gemming, B. Montanari, N. M. Harrison, B. Buchner, and G. A. D. Briggs, Nature Nanotech. **4**, 500 (2009).
[25]L. Sun, F. Banhart, A. V. Krasheninnikov, J. A. Rodríguez-Manzo, M. Terrones, and P. M. Ajayan, Science **312**, 1199 (2006).
[26]L. Sun, A. V. Krasheninnikov, T. Ahlgren, K. Nordlund, and F. Banhart, Phys. Rev. Lett. **101**, 156101 (2008).
[27]A. J. Stone and D. J. Wales, Chem. Phys. Lett. **128**, 501 (1986).
[28]N. Metropolis, A. E. Rosenbluth, M. N. Rosenbluth, A. H. Teller, and E. Teller, J. Chem. Phys. **21**, 1087 (1953).
[29]G. Kresse and J. Furthmuller, *VASP The Guide* (Vienna University of Technology, Vienna, 2001).
[30]J. P. Perdew and Y. Wang, Phys. Rev. B **45**, 13244 (1992).
[31]D. Vanderbilt, Phys. Rev. B **41**, 7892 (1990).
[32]H. J. Monkhorst and J. D. Pack, Phys. Rev. B **13**, 5188 (1976).
[33]V. Perebeinos and J. Tersoff, Phys. Rev. B **79**, 241409 (2009).
[34]R. C. Haddon, J. Am. Chem. Soc. **112**, 3385 (1990); R. C. Haddon, Acc. Chem. Res. **21**, 243 (1988).
[35]R. C. Haddon, L. E. Brus, and K. Raghavachari, Chem. Phys. Lett. **125**, 459 (1986); R. C. Haddon, L. E. Brus, and K. Raghavachari, *ibid*. **131**, 165 (1986) R. C. Haddon, J. Am. Chem. Soc. **108**, 2837 (1986).
[36]M. A. Hamon, M. E. Itkis, S. Niyogi, T. Alvaraez, C. Kuper, M. Menon, and R. C. Haddon, J. Am. Chem. Soc. **123**, 11292 (2001).
[37]F. Wooten, K. Winer, and D. Weaire, Phys. Rev. Lett. **54**, 1392 (1985).
[38]E. Polak, *Computational Methods in Optimization* (Academic, New York, 1971).
[39]C. P. Ewels, M. I. Heggie, and P. R. Briddon, Chem. Phys. Lett. **351**, 178 (2002).
[40]L. Li, S. Reich, and J. Robertson, Phys. Rev. B **72**, 184109 (2005).
[41]D. W. Brenner, Phys. Rev. B **42**, 9458 (1990).
[42]J. C. Meyer, C. Kisielowski, R. Erni, M. D. Rossell, M. F. Crommie, and A. Zettl, Nano Lett. **8**, 3582 (2008).
[43]C. Piskoti, J. Yarger, and A. Zettl, Nature **393**, 771 (1998).
[44]H. W. Kroto, J. R. Heath, S. C. O'Brien, R. F. Curl, and R. E. Smalley, Nature **318**, 162 (1985).
[45]F. Diederich and R. L. Whetten, Acc. Chem. Res. **25**, 119 (1992).
[46]H. W. Kroto, Nature **329**, 529 (1987).
[47]T. G. Schmalz, W. A. Seitz, D. J. Klein, and G. E. Hite, J. Am. Chem. Soc. **110**, 1113 (1988).
[48]J. G. Kushmeric, K. F. Kelly, H.-P. Rust, N. J. Halas, and P. S. Weiss, J. Phys. Chem. B **103**, 1619 (1999).
[49]J. R. Hahn and H. Kang, Phys. Rev. B **60**, 6007 (1999).
[50]A. V. Krasheninnikov and K. J. Nordlund, J. Vac. Sci. Technol. B **20**, 728 (2002).
[51]A. A. El-Barbary, R. H. Telling, C. P. Ewels, M. I. Heggie, and P. R. Briddon, Phys. Rev. B **68**, 144107 (2003).
[52]M. H. Gass, U. Bangert, A. L. Bleloch, P. Wang, R. R. Nair, and A. K. Geim, Nature Nanotechnol. **3**, 676 (2008).
[53]For a single vacancy in graphene, for instance, removal of one C atom is followed by symmetry-lowering lattice relaxation that causes two neighboring atoms to form a weak covalent bond. The remaining unsaturated C atom protrudes out of plane, due in part to the repulsion between the unpaired and paired electrons. With penalty energy of about 2.6 eV per dangling bond, the VFF model tends to provide a good match with the calculated DFT vacancy formation energy; however, more sophisticated potential models are needed in order to accurately describe the nature of bond-coordination defects such as weak bond formation.